

Constrained Physics-Informed Deep Learning for Stable System Identification and Control of Unknown Linear Systems

Ján Drgoňa, Aaron Tuor, Draguna Vrabie
Pacific Northwest National Laboratory
Richland, Washington USA
{jan.drgona, aaron.tuor, draguna.vrabie}@pnnl.gov

Abstract

This paper presents a novel data-driven method for learning deep constrained continuous control policies and dynamical models of linear systems. By leveraging partial knowledge of system dynamics and constraint enforcing multi-objective loss functions, the method can learn from small and static datasets, handle time-varying state and input constraints and enforce the stability properties of the controlled system. We use a continuous control design example to demonstrate the performance of the method on three distinct tasks: system identification, control policy learning, and simultaneous system identification and policy learning. We assess the system identification performance by comparing open-loop simulations of the true system and the learned models. We demonstrate the performance of the policy learning methodology in closed-loop simulations using the system model affected by varying levels of parametric and additive uncertainties. We report superior performance in terms of reference tracking, robustness, and online computational and memory footprints compared with classical control approaches, namely LQR and LQI controllers, and with three variants of model predictive control (MPC) formulations and two traditional MPC solution approaches. We then evaluate the potential of simultaneously learning the system model and control policy. Our empirical results demonstrate the effectiveness of our unifying framework for constrained optimal control of linear systems to provide stability guarantees of the learned dynamics, robustness to uncertainty, and high sampling efficiency.

and constrained operating regimes. This presents challenges to design efficient and robust control algorithms. Advanced control design requires expertise in applied mathematics, dynamic systems theory, computational methods, mathematical modeling, optimization frameworks, and operator assisted algorithmic tuning of control parameters. These requirements increase cost and reduce their applicability only to high value systems where marginal operational performance improvements lead to huge economic benefits.

Data-driven dynamics modeling and control policy learning show promise to “democratize” advanced control to systems with complex and partially characterized dynamics. However, pure data-driven methods typically suffer from poor-sampling efficiency, scale poorly with problem size, and exhibit slow convergence to optimal decisions [24]. Of special concern are lack of guarantees that black-box data-driven controllers will obey operational constraints and may occlude understanding of general system operation and diagnosis of potential failure modes.

Contributions: In this work we aim to embed domain knowledge into modern AI-based data-driven decision systems. We develop a hybrid framework which integrates linear dynamic systems and control theory with recent advances in deep learning. The framework is based on neural parametrization of the closed loop dynamical system with two building blocks: i) neural system model conditioned by known properties of the physical system, and ii) a deep learning formulation of model predictive control policy. In particular, we combine system identification based on constrained recurrent neural networks with eigenvalue regularization on the layer weights, and policy optimization with embedded inequality constraints via backpropagation of the control loss through the linear system model. To the authors’ best knowledge this is the first time these methods have been used in conjunction in the single study.

1. Introduction

Many real-world systems of critical interest have unknown dynamics, uncertain and dynamic operating environments,

We apply these methods to system identification and control policy learning for a linear control problem representative of building temperature dynamics and demonstrate that: i) embedding constraints provides advantages of sample ef-

efficiency, and physically plausible outcomes, ii) eigenvalue regularizations guarantee the stability and invertibility of the learned model, iii) in terms of control performance and robustness, our deep learning control policies outperform classical control approaches, namely LQR, and LQI controllers, as well as robust and stochastic MPC formulations during simulations affected by parametric and additive uncertainties, and iv) the presented methods are more computationally and memory efficient than traditional MPC solutions based on online constrained optimization or offline multi-parametric programming.

1.1. Related Work

Stable neural architectures: There has recently been intense research on the *stability of deep learning layers*. The IMEXnet constrains the eigenvalues of the network Jacobians by bounding the layer weights [29]. Stability around equilibrium point and nominal trajectory for a dynamical system controlled by neural network was studied in [37]. Joint learning of the Lyapunov functions was proved to guarantee the stability of the learned system dynamics and control policies [42, 57]. Authors in [28] linked the vanishing and exploding gradient problems with the stability of the neural networks interpreted as ODEs and proposed restricted architecture with guaranteed stability. Our own work follows this tradition, presenting a new RNN parametrization with guaranteed bounds on the dominant eigenvalues of the transition matrices. Theoretical foundations of the used constraints and stability regularizations of the proposed method are inspired by interpretations of deep neural networks through the optics of differential equations [32, 17, 48, 29], and neural architectures based on physics priors such as Hamiltonian [26] and Lagrangian [49] networks.

System identification with neural networks: The natural idea of using RNN-based state-space models is motivated by previous works [44, 43, 56, 30]. A related idea of using convex-based LSTM networks for faster converging system identification of control-oriented dynamical models was presented in [66]. The use of the linear dynamics is motivated by the possibility of a straightforward extension to nonlinear systems via Hammerstein-Wiener RNN structure composed of a dynamic linear subsystem embedded between two static nonlinear subsystems holding the universal approximation theorem [38]. Alternative, but related approach of incorporating prior structural knowledge is the use graph neural networks, which have been recently demonstrated to simulate complex physical systems with state-of-the-art performance across a variety of physical domains [58, 59, 60]. In comparison with the referenced approaches, the novel features of the proposed modeling method are the use of novel eigenvalue regularization of the layer weights to guarantee the stability of the unrolled dy-

namics and the use of penalty methods to impose inequality constraints over the state space, applicable beyond simple linear systems.

Model-based optimal control: One of the main motivations of the presented paper is to develop a competitive method for the design of constrained optimal controllers for linear systems which would outperform the classical approaches such as LQR, or model predictive control (MPC) based on constrained optimization [27, 51]. The structure of the control agent in this work is inspired by the formulation of MPC problem using barrier functions [65]. Such that, optimizing the proposed deep learning based policy for a single measurement is equivalent with solving constrained MPC via penalty methods. However, the main difference comparing with MPC and LQR is that the proposed method does not require the system model beforehand and can jointly optimize both system models as well as explicit control policy. Moreover, compared to unconstrained LQR, the method can handle inequality constraints similarly to MPC. In the field of MPC, as an alternative to solving the corresponding constrained optimization problem online, the solution can be pre-computed offline using multiparametric programming (mpP) [45] and obtain so-called explicit MPC (eMPC) policy [9, 63]. The benefits of eMPC are typically faster online computations, exact bounds on worst-case execution time, and simple and verifiable policy code, which makes it a suitable approach for embedded applications. However, eMPC suffer from the well-known curse of dimensionality which severely limits its practical applicability only to small scale systems with short prediction horizons [2]. The presented method represents a scalable alternative, using deep learning to approximate the explicit MPC policy for linear systems given state and input constraints without the exponential blow up in the problem complexity.

Adaptive and learning-based MPC: The proposed methods are closely related to learning-based MPC (LBMPC) methods, introduced by [6], leveraging machine learning methods for learning the prediction model from data. In general, LBMPC is considered to be a generalization of robust adaptive MPC, which is typically restricted to specific types of model structures and learning algorithms [7]. To make LBMPC tractable, the performance and safety tasks are decoupled by using reachability analysis [5, 55]. Alternatives include formulation of robust MPC with state-dependent uncertainty for data-driven linear models [62], or iterative model updates for linear systems with bounded additive uncertainty and robust guarantees [14]. For a comprehensive review of LBMPC approaches we refer the reader to a recent review [36] and references therein. The idea of backpropagating through the learned system model parametrized via convex neural networks [3] was investigated in [18]. However, in all of the aforementioned

LBMPC approaches, the control policy is defined implicitly by the solver and requires the online solution of the constrained optimization problem. While in the proposed methodology, the policy is learned offline from measurement data and hence generates MPC policy parametrized explicitly by a neural network.

Imitation learning of MPC: The related methods combining data-driven and classical model-based approaches include learning MPC policies from simulation data using deep learning [39, 67], learning control policies with constraint handling capabilities [35, 68, 16, 69], learning MPC solutions using Autoencoders [64], and representing MPC or LQR optimization problems as layers in deep networks [4, 1]. However, all of these approaches fall into the category of imitation learning, which requires the training data to be generated by the original MPC. In contrast, the presented method represent off-policy optimization, which does not require the supervisory control policy nor system model beforehand and learns both from the measurement data.

Model-based reinforcement learning: From *reinforcement learning-based control* perspective, the complexity of constrained sequential decision making with continuous control actions represents one of the main challenges in the domain [24]. Several advances have been made by leveraging high-fidelity solutions obtained by trajectory optimization to speed up the training of neural network controllers [52, 67], learning deep inverse dynamics models [19], or by learning deep neural network representations of the underlying system dynamics to be used by MPC [11, 13]. Conceptually similar control frameworks with differentiable physical models have been introduced for the robotics domain with the emphasis on the rigid body dynamics [21, 22]. There are also similarities with stochastic value gradients (SVG) learning continuous control policies using backpropagation [33]. Jointly learning the system dynamics model and control policies from pixels by backpropagating through the learned model was presented by the RL framework called Dreamer [31]. Similarly, the presented deep learning-based MPC approach is based on backpropagation through the learned system model. However, in contrast with the referenced approaches dealing with nonlinear systems and visual feedback systems, the ambition of this paper is to present a competitive alternative to widely used linear MPC approaches. We achieve this by superior robustness to uncertainties, and by overcoming the computational challenges of associated explicit solutions.

2. Methods

We describe the application of our control design methods to a dynamical system. Section 2.1 describes three

parametrized RNN models designed for system identification, and our contribution of a RNN constructed to enforce the stability and well-posedness of the learning problem. Section 2.2 provides a brief overview of model predictive control, while section 2.3 describes our reformulation of MPC as a deep learning optimization problem. We conclude the Methods section with a description of our algorithm for constrained control policy learning and joint system identification and policy learning.

We choose a classical linear time invariant state space model for the ground truth dynamics:

$$\mathbf{x}_{k+1} = \mathbf{A}\mathbf{x}_k + \mathbf{B}\mathbf{u}_k + \mathbf{E}\mathbf{d}_k \quad (1)$$

where $\mathbf{x}_k \in \mathbb{R}^{n_x}$ is the system state, $\mathbf{u}_k \in \mathbb{R}^{n_u}$ is the control input, and $\mathbf{d}_k \in \mathbb{R}^{n_d}$ is disturbance at time k .

2.1. System Identification

From a physical systems perspective, we can think of the layers of a recurrent neural network (RNN) as dynamical transformations acting on system state variables describing their causal interactions. The parametrized dynamical system model can be encoded by a recurrent neural network:

$$\mathbf{x}_{k+1} = f(\mathbf{x}_k, \mathbf{u}_k, \mathbf{d}_k) \quad (2)$$

Using the notation from classical control, \mathbf{x}_k corresponds to the hidden state of the RNN at time step k , whereas $[\mathbf{u}_k \ \mathbf{d}_k] \in \mathbb{R}^{n_u+n_d}$, the concatenation of \mathbf{u}_k and \mathbf{d}_k , is considered the input to the network at time k . In this work we experiment with four state transition functions, f_{LIN} , f_{RNN} , f_{GRU} , and f_{SSM} , for a simple unconstrained linear model, a standard recurrent neural network with Rectified Linear Unit (ReLU) activation, Gated Recurrent Unit [20], and our customized state space model designed to maintain known characteristics of the system through implicit eigenvalue constraints.

Standard models: The linear model is the same form as the true system but with learned parameters $\tilde{\mathbf{A}}$, $\tilde{\mathbf{B}}$, and $\tilde{\mathbf{E}}$:

$$f_{\text{LIN}}(\mathbf{x}, \mathbf{u}, \mathbf{d}) = \tilde{\mathbf{A}}\mathbf{x} + \tilde{\mathbf{B}}\mathbf{u} + \tilde{\mathbf{E}}\mathbf{d} \quad (3)$$

The standard RNN is defined as:

$$f_{\text{RNN}}(\mathbf{x}, \mathbf{u}, \mathbf{d}) = \text{ReLU}(\tilde{\mathbf{A}}\mathbf{x} + [\tilde{\mathbf{B}} \ \tilde{\mathbf{E}}] [\mathbf{u} \ \mathbf{d}]^T) \quad (4)$$

where $\tilde{\mathbf{A}}$, and $[\tilde{\mathbf{B}} \ \tilde{\mathbf{E}}]$ correspond to the hidden and input weights respectively. The block matrix notation shows that the standard formulation of an RNN can be decomposed into a structure corresponding to the linear system since $[\tilde{\mathbf{B}} \ \tilde{\mathbf{E}}] [\mathbf{u} \ \mathbf{d}]^T = \tilde{\mathbf{B}}\mathbf{u} + \tilde{\mathbf{E}}\mathbf{d}$.

While the GRU does not have a similar correspondence to the physical system, we include this architecture for compar-

ison with a popular deep learning architecture with demonstrated success in sequential modeling tasks. So,

$$\mathbf{w} = \sigma(\tilde{\mathbf{B}}_1 \mathbf{u} + \tilde{\mathbf{E}}_1 \mathbf{d} + \tilde{\mathbf{A}}_1 \mathbf{x}) \quad (5)$$

$$\mathbf{n} = \tanh(\tilde{\mathbf{B}}_2 \mathbf{u} + \tilde{\mathbf{E}}_2 \mathbf{d} + \mathbf{w} \odot \tilde{\mathbf{A}}_2 \mathbf{x}) \quad (6)$$

$$\mathbf{z} = \sigma(\tilde{\mathbf{B}}_3 \mathbf{u} + \tilde{\mathbf{E}}_3 \mathbf{d} + \tilde{\mathbf{A}}_3 \mathbf{x}) \quad (7)$$

$$f_{\text{GRU}}(\mathbf{x}, \mathbf{u}, \mathbf{d}) = (\mathbf{1} - \mathbf{z}) \odot \mathbf{n} + \mathbf{z} \odot \mathbf{x} \quad (8)$$

where σ , the element-wise logistic sigmoid, creates gating matrices \mathbf{w} and \mathbf{z} , and \odot is the Hadamard product.

Stability, invertibility and well-posedness: By the Perron–Frobenius theorem [41], the dominant eigenvalue of a non-negative square matrix \mathbf{A} is bounded by the minimum and maximum of its row-wise sums. That is, there exists a real eigenvalue of \mathbf{A} , $\rho > 0$ s.t. for any other eigenvalue, λ , $|\lambda| < \rho$, and $\min_i \sum_j A_{ij} \leq \rho \leq \max_i \sum_j A_{ij}$. Hence, one can enforce bounds on dominant eigenvalue by constraining the row-wise sums of \mathbf{A} ’s elements. Let σ be the elementwise standard logistic sigmoid function, $\epsilon \in [0, 1]$, and $\mathbf{1}$ a matrix of 1’s. Our parametrization, bounding the dominant eigenvalue of the transition matrix $\tilde{\mathbf{A}}$ to $\rho \in [1 - \epsilon, 1]$, is formulated as:

$$\mathbf{M} = \mathbf{1} - \epsilon \sigma(\mathbf{M}') \quad (9)$$

$$\tilde{\mathbf{A}}_{i,j} = \frac{\exp(\tilde{\mathbf{A}}'_{ij}) \mathbf{M}_{i,j}}{\sum_{k=1}^{n_x} \exp(\tilde{\mathbf{A}}'_{ik})} \quad (10)$$

$$f_{\text{SSM}}(\mathbf{x}_k, \mathbf{u}_k, \mathbf{d}_k) = \tilde{\mathbf{A}} \mathbf{x}_k + \tilde{\mathbf{B}} \mathbf{u}_k + \tilde{\mathbf{E}} \mathbf{d}_k \quad (11)$$

\mathbf{M} is a matrix modeling damping defined as a function of parameter matrix $\mathbf{M}' \in \mathbb{R}^{n_x \times n_x}$. \mathbf{M} ’s elementwise multiplication with the softmax regularized rows of the $\tilde{\mathbf{A}}$ ’ matrix gives the state transition matrix $\tilde{\mathbf{A}}$. By constraining the magnitudes of the dominant eigenvalue to be less or equal to one, the stability of the learned dynamics of the discrete system is guaranteed. As pointed out in [28], by enforcing eigenvalues of the layer weights to be close to one (zero for continuous-time systems), the learning problem is well-posed as it prevents exploding and vanishing gradients even for very deep networks. Moreover, the stable eigenvalue regularizations favor learning invertible layers as shown by the study on iResNets [8] linking the layer invertibility with the eigenvalues of the layer’s Jacobians. Under certain conditions, the stability guarantees also generalize to non-linear layers. In particular, the stability holds as long as the dominant eigenvalue is bounded from above by one, and all network activation functions f have bounded maximum value of their derivative less or equal to one, $\max(f'(x)) \leq 1$. However, the exact dominant eigenvalue constraint will be conserved only if $\max(f'(x)) = 1$. This property is satisfied by a number of prospective nonlinear activation functions, e.g., $\max(\text{ReLU}'(x)) = 1$, $\max(\text{leakyReLU}'(x)) = 1$, $\max(\arctan'(x)) = 1$, and $\max(\sigma'(4x)) = 1$. As alternative extension to nonlinear dynamics, we propose the use

of the given eigenvalue regularization on the linear units of the Hammerstein-Weiner RNN models [38]. A potential disadvantage of the parametrization is the layer weights are restricted to be positive, which may be an unsuitable restriction for some applications. On the other hand, this parametrization is a suitable choice for modeling of a wide class of dissipative dynamical system if $\epsilon > 0$, systems conserving the energy if $\epsilon = 0$, or non-dissipative (unstable) systems if we allow $\epsilon < 0$.

Model optimization: For the given recurrent neural network models we optimize the corresponding $\tilde{\mathbf{A}}$, $\tilde{\mathbf{B}}$, $\tilde{\mathbf{E}}$ (and \mathbf{M}' for SSM) parameter matrices by an objective function which serves as a reasonable proxy for our goal to reproduce the response of the original system. We use the average Mean Squared Error (MSE) for the model response over an N -step prediction horizon compared to data obtained from the ground truth system dynamics (1). For each N time steps simulation of the ground truth system we have sequences of vectors, $\mathcal{X}^{\text{ID}} = \mathbf{x}_0^{\text{ID}}, \dots, \mathbf{x}_N^{\text{ID}}$, $\mathcal{U}^{\text{ID}} = \mathbf{u}_0^{\text{ID}}, \dots, \mathbf{u}_N^{\text{ID}}$, $\mathcal{D} = \mathbf{d}_0, \dots, \mathbf{d}_N$. The model is given only an initial state \mathbf{x}_0^{ID} , and system inputs \mathcal{U}^{ID} , and disturbances \mathcal{D} are provided to loop over the model and produce a sequence of state predictions, $\tilde{\mathcal{X}} = \tilde{\mathbf{x}}_0, \dots, \tilde{\mathbf{x}}_N$. We assume that for optimization we only have access to one observable variable from the complete state denoted by index i . The loss function is the mean squared error (MSE) between our state prediction and that of the true system:

$$\mathcal{L}_{\text{MSE}}(\tilde{\mathcal{X}}, \mathcal{X}^{\text{ID}} | \tilde{\mathbf{A}}, \tilde{\mathbf{B}}, \tilde{\mathbf{E}}) = \frac{1}{N} \sum_{k=1}^N \|\tilde{\mathbf{x}}_{k,i} - \mathbf{x}_{k,i}^{\text{ID}}\|_2^2 \quad (12)$$

We optimize the models implemented¹ in the Pytorch deep learning library [53] using the AdamW [47] variant of full-batch gradient descent.

2.2. Model Predictive Control

Model predictive control (MPC) is an optimal control strategy that calculates the control inputs trajectories by minimizing a given objective function over a finite prediction horizon with respect to the constraints on the system dynamics. Let us consider a reference tracking MPC, formulated as the following constrained optimization problem:

$$\min_{u_0, \dots, u_{N-1}} \sum_{k=0}^{N-1} (\|\mathbf{x}_k - \mathbf{r}_k\|_{Q_r}^2 + \|\mathbf{u}_k\|_{Q_u}^2) \quad (13a)$$

$$\text{s.t. } \mathbf{x}_{k+1} = f(\mathbf{x}_k, \mathbf{u}_k, \mathbf{d}_k), \quad k \in \mathbb{N}_0^{N-1} \quad (13b)$$

$$g(\mathbf{x}_k) \leq \mathbf{0}, \quad k \in \mathbb{N}_0^{N-1} \quad (13c)$$

$$h(\mathbf{u}_k) \leq \mathbf{0}, \quad k \in \mathbb{N}_0^{N-1} \quad (13d)$$

$$\mathbf{x}_0 = \mathbf{x}(t), \quad (13e)$$

¹Code for reproducing our experiments is available at: https://github.com/pnnl/deps_arXiv2020

where $\mathbb{N}_a^b = \{a, a+1, \dots, b\}$ is a set of integers. The predictions are obtained from the system model differential equations (13b) over the prediction horizon N . The system is also subject to state (13c) and input (13d) constraints. The objective function (13a) is the weighted squared 2-norm i.e., $\|\mathbf{a}\|_Q^2 = \mathbf{a}^T Q \mathbf{a}$, and penalizes the distance of the states from references, while minimizing the control effort.

The constrained optimization problem (13) can be reformulated using barrier functions [12, 10] as the following unconstrained optimization problem in a generic form:

$$\min_{u_0, \dots, u_{N-1}} \sum_{k=0}^{N-1} (\ell(\mathbf{x}_k, \mathbf{r}_k, \mathbf{u}_k) + \lambda \sum_{i=1}^m p_x(g_i(\mathbf{x}_k)) + \mu \sum_{j=1}^n p_u(h_j(\mathbf{u}_k))), \quad (14)$$

where $\ell(\bullet)$ defines the loss function, while λ and μ define weights of a barrier functions p_x and p_u associated with state (13c) and input (13d) constraints, where integers m and n specify the number of constraints.

2.3. Physics-informed Control Policy Architecture

We use the parametrized dynamical model of the system (2) as an integral part of the policy architecture. The control-oriented loss function is backpropagated through the differentiable model to update the policy parameters. The model serves as an internal simulator for the imagination of different possible outcomes of the control actions and environment conditions. A crucial part of the policy are inequality constraints modeled as barrier penalties to ensure the safety of the policy. The main challenge here is to parametrize the MPC problem (13) as a deep learning model while preserving the structure of the original problem.

Modeling of equality constraints: We use the recurrent encoding of equality constraints, also called a single shooting formulation [27]. Here the length of the prediction horizon N defines the number of steps to unroll the dynamical model (2) for backpropagation through time [54].

Modeling of inequality constraints: We exploit the possibility of reformulating the constrained optimization problem (13) into the unconstrained from (14) by the barrier method. We use ReLU units to model the violations of time-varying inequality constraints as follows:

$$\underline{\mathbf{x}}_k \leq \mathbf{x}_k + \mathbf{s}_k^x \cong \mathbf{s}_k^x = \text{ReLU}(-\mathbf{x}_k + \underline{\mathbf{x}}_k), \quad (15a)$$

$$\mathbf{x}_k - \mathbf{s}_k^x \leq \bar{\mathbf{x}}_k \cong \mathbf{s}_k^x = \text{ReLU}(\mathbf{x}_k - \bar{\mathbf{x}}_k). \quad (15b)$$

Slack variables \mathbf{s}_k^u and \mathbf{s}_k^x represent the violations of the inequality constraints and correspond to the barrier function terms in the objective (14), with large penalties λ and μ .

Modeling of control policy layers: The choice of the layer of control policy $\mathbf{u}_k = \phi(\xi|\Theta)$ depends on the problem complexity. For the purposes of this paper we used a two-layer neural network with ReLU activations.

2.4. Constrained Control Policy Learning

We use the system model as an integral part of learning the policy. The constrained control policy is equivalent to the constraints of the problem (13) and can be defined as the following algorithm 1. The control policy is evaluated on line 3. The violations of the control constraints are computed on lines 4, 5, and 6, respectively. In line 7, the system model is integrated forward in time to simulate the evolution of the states. The state constraints are evaluated on lines 8, 9, and 10, respectively. And finally, the forward pass of the policy returns computed control actions, predicted states, and slacks representing constraints violations.

Algorithm 1 Constrained model predictive control policy

```

1: function MPCPOLICY( $\mathbf{x}_k, \mathbf{d}_k, \mathbf{r}_k, \underline{\mathbf{x}}_k, \bar{\mathbf{x}}_k, \mathbf{u}_k, \bar{\mathbf{u}}_k$ )
2:    $\xi = \{\mathbf{x}_k, \mathbf{d}_k, \mathbf{r}_k, \underline{\mathbf{x}}_k, \bar{\mathbf{x}}_k, \mathbf{u}_k, \bar{\mathbf{u}}_k\}$   $\triangleright$  policy inputs
3:    $\mathbf{u}_k = \phi(\xi|\Theta)$   $\triangleright$  policy evaluation
4:    $\mathbf{s}_k^u = \text{ReLU}(-\mathbf{u}_k + \underline{\mathbf{u}}_k)$   $\triangleright$  control lower bound
5:    $\mathbf{s}_k^u = \text{ReLU}(\mathbf{u}_k - \bar{\mathbf{u}}_k)$   $\triangleright$  control upper bound
6:    $\mathbf{s}_k^u = \mathbf{s}_k^u + \mathbf{s}_k^u$   $\triangleright$  control constraints violations
7:    $\tilde{\mathbf{x}}_{k+1} = f(\mathbf{x}_k, \mathbf{u}_k, \mathbf{d}_k)$   $\triangleright$  state update
8:    $\mathbf{s}_k^x = \text{ReLU}(-\tilde{\mathbf{x}}_{k+1} + \underline{\mathbf{x}}_k)$   $\triangleright$  state lower bound
9:    $\mathbf{s}_k^x = \text{ReLU}(\tilde{\mathbf{x}}_{k+1} - \bar{\mathbf{x}}_k)$   $\triangleright$  state upper bound
10:   $\mathbf{s}_k^x = \mathbf{s}_k^x + \mathbf{s}_k^x$   $\triangleright$  state constraints violations
11:  return  $\mathbf{u}_k, \tilde{\mathbf{x}}_{k+1}, \mathbf{s}_k^x, \mathbf{s}_k^u$ 
12: end function

```

To populate the training dataset for learning the robust control policy, initial states, references, and disturbances are randomly initialized within realistic operating ranges. An alternative choice of the training data can be obtained from typical trajectories of the controlled system, e.g., from measurements or specified by a domain expert. For each N samples we thus have sequence of vectors $\mathcal{X} = \mathbf{x}_0, \dots, \mathbf{x}_N$, $\mathcal{R} = \mathbf{r}_0, \dots, \mathbf{r}_N$, and $\mathcal{D} = \mathbf{d}_0, \dots, \mathbf{d}_N$. The trainable parameters Θ of the MPCPOLICY are optimized w.r.t. the following weighted multi-objective loss function:

$$\mathcal{L}_{\text{MSE}}(\mathcal{X}, \mathcal{D}, \mathcal{R}, \text{MPCPOLICY}|\Theta) = \frac{1}{N} \sum_{k=0}^{N-1} (Q_r \|\mathbf{r}_{k+1} - \tilde{\mathbf{x}}_{k+1}\|_2^2 + Q_u \|\mathbf{u}_k\|_2^2 + \lambda \|\mathbf{s}_k^x\|_2^2 + \mu \|\mathbf{s}_k^u\|_2^2). \quad (16)$$

Where, the first term stands for the reference tracking loss, the second term penalizes the square of the control actions, while the last two terms penalize the constraints violations. The relative importance of the individual terms is balanced by weight factors Q_r , Q_u , λ , and μ .

2.5. Joint System Identification and Control Learning

The aim here is to learn a system model alongside the control policy. The modified policy is defined by algorithm 2. In algorithm 1 the true system dynamics are available, whereas in algorithm 2 the system model is learned alongside the control policy. The policy learning loss function (16) is extended with a system identification term penalizing model deviations from measured states with weight Q_{ID} , and with state trajectory smoothening term weighted with $Q_{\Delta x}$ as follows:

$$\begin{aligned} \mathcal{L}_{\text{MSE}}(\mathcal{X}^{\text{ID}}, \mathcal{U}^{\text{ID}}, \mathcal{X}, \mathcal{D}, \mathcal{R}, \text{IDPOLICY}|\Theta) = \\ \frac{1}{N} \sum_{k=0}^{N-1} (Q_r \|\mathbf{r}_{k+1} - \tilde{\mathbf{x}}_{k+1}\|_2^2 + Q_u \|\mathbf{u}_k\|_2^2 + \lambda \|\mathbf{s}_k^x\|_2^2 \\ + \mu \|\mathbf{s}_k^u\|_2^2 + Q_{ID} \|\mathbf{x}_{k+1}^{\text{ID}} - \tilde{\mathbf{x}}_{k+1}^{\text{ID}}\|_2^2 + Q_{\Delta x} \|\Delta \mathbf{x}_k^{\text{ID}}\|_2^2) \end{aligned} \quad (17)$$

In algorithm 2, we simulate the system model for the control and modeling tasks in parallel trajectories on lines 7, and 8. \mathcal{X}^{ID} , as defined in section 2.1, is used to calculate loss for updating the parameters of the internal model on line 8. On other hand, \mathcal{X} as defined in section 2.4 is used to initialize the internal model on line 7 for the control policy update. Analogously, \mathcal{U}^{ID} , and \mathcal{U} are control input trajectories associated with the system model and policy updates, respectively. To increase the smoothness of learned trajectories, line 9 defines the state residual to be minimized during the training. Gradient updates are performed jointly on the aggregate loss (17) associated with the parallel system identification and control policy trajectories.

Algorithm 2 Joined model and control policy learning

```

1: function IDPOLICY( $\mathbf{x}_k^{\text{ID}}, \mathbf{u}_k^{\text{ID}}, \mathbf{x}_k, \mathbf{d}_k, \mathbf{r}_k, \mathbf{x}_k, \bar{\mathbf{x}}_k, \mathbf{u}_k, \bar{\mathbf{u}}_k$ )
2:    $\xi = \{\mathbf{x}_k, \mathbf{d}_k, \mathbf{r}_k, \mathbf{x}_k, \bar{\mathbf{x}}_k, \mathbf{u}_k, \bar{\mathbf{u}}_k\}$   $\triangleright$  policy inputs
3:    $\mathbf{u}_k = \phi(\xi|\Theta)$   $\triangleright$  control policy evaluation
4:    $\mathbf{s}_k^u = \text{ReLU}(-\mathbf{u}_k + \bar{\mathbf{u}}_k)$   $\triangleright$  control lower bound
5:    $\mathbf{s}_k^{\bar{u}} = \text{ReLU}(\mathbf{u}_k - \bar{\mathbf{u}}_k)$   $\triangleright$  control upper bound
6:    $\mathbf{s}_k^u = \bar{\mathbf{s}}_k^u + \mathbf{s}_k^u$   $\triangleright$  control constraints violations
7:    $\tilde{\mathbf{x}}_{k+1} = f(\mathbf{x}_k, \mathbf{u}_k, \mathbf{d}_k)$   $\triangleright$  control state update
8:    $\tilde{\mathbf{x}}_{k+1}^{\text{ID}} = f(\mathbf{x}_k^{\text{ID}}, \mathbf{u}_k^{\text{ID}}, \mathbf{d}_k)$   $\triangleright$  system ID state update
9:    $\Delta \mathbf{x}_k^{\text{ID}} = \tilde{\mathbf{x}}_{k+1}^{\text{ID}} - \mathbf{x}_{k+1}^{\text{ID}}$   $\triangleright$  system ID state residual
10:   $\mathbf{s}_k^x = \text{ReLU}(-\tilde{\mathbf{x}}_{k+1} + \mathbf{x}_k)$   $\triangleright$  state lower bound
11:   $\mathbf{s}_k^{\bar{x}} = \text{ReLU}(\tilde{\mathbf{x}}_{k+1} - \mathbf{x}_k)$   $\triangleright$  state upper bound
12:   $\mathbf{s}_k^x = \bar{\mathbf{s}}_k^x + \mathbf{s}_k^x$   $\triangleright$  state constraints violations
13:  return  $\mathbf{u}_k, \tilde{\mathbf{x}}_{k+1}, \mathbf{s}_k^x, \mathbf{s}_k^u, \tilde{\mathbf{x}}_{k+1}^{\text{ID}}, \Delta \mathbf{x}_k^{\text{ID}}$ 
14: end function

```

A key added value to classical control techniques is that, in addition to the control policy, the system model can adapt to possibly shifting ground truth system dynamics. Upon deployment, to grant the policy added adaptive behavior, we introduce a feedback term $\mathbf{x}_k = \mathbf{x}_k + \hat{\mathbf{x}}_k$ with learnable

parameter $\hat{\mathbf{x}}_k$, allowing the model to update the state initial conditions online during closed-loop control. The system model update runs the optimization for a limited number of epochs at each sampling instant using the current sample of measured values $\mathbf{x}_k^{\text{ID}}, \mathbf{u}_k^{\text{ID}}, \mathbf{x}_k, \mathbf{d}_k, \mathbf{r}_k, \mathbf{x}_k, \bar{\mathbf{x}}_k, \mathbf{u}_k, \bar{\mathbf{u}}_k$. To avoid catastrophic forgetting due to learning on a small sample, we fix the model parameters and update only the last layer of the policy $\mathbf{u}_k = \phi(\xi|\Theta)$ and only the state correction term $\hat{\mathbf{x}}_k$. In this way the policy and the system models can adapt to new data while preserving most of the learned dynamics from the offline learning phase.

3. Numerical Case Studies

In this section we present the dataset, metrics, experimental set-ups, results, and analyses for experiments with our system identification and control policy learning methods.

3.1. System model

The case study is based on the thermal model of a building in the form of (1). The states $\mathbf{x}_k \in \mathbb{R}^4$ represent wall ($x_{k,1}$), ceiling ($x_{k,2}$), floor ($x_{k,3}$), and room temperature ($x_{k,4}$, the observed state), respectively. Control inputs \mathbf{u} represent heat flow delivered to the building by the radiator. While measured disturbances $\mathbf{d}_k \in \mathbb{R}^3$ represent ambient temperature ($\mathbf{d}_{k,1}$), solar irradiation ($\mathbf{d}_{k,2}$), and internal heat gains ($\mathbf{d}_{k,3}$), respectively. In practice, real-time updates of \mathbf{d} are obtained from weather forecast. An interesting property of the thermal models is that their transition matrix $\hat{\mathbf{A}}$ is non-negative with stable eigenvalues. This property motivates the eigenvalue regularization given by (10), where the damping factor \mathbf{M} constrains the dissipation of the system and can be physically interpreted as heat losses of the building structure. Hence physical insights can be used for tuning of the proposed model to different building types. The penalty constraints on the state trajectories are inspired by the physically meaningful values and are chosen to demonstrate a tutorial control example, which requires balancing a multi-term objective function. Even though the selected values of the inequality and eigenvalue constraints have been inspired by this particular physical process, the underlying modeling principles are generic and could be applied to various types of systems.

3.2. Dataset

System identification: The objective of the system identification task is to identify the parameters of the unknown linear system given the measurement data. Our experimental dataset is constructed by simulating the true system dynamic model (1), generating the state trajectories \mathcal{X}^{ID} with initial conditions of $x_0 = 20^\circ\text{C}$. The initial control policy is assumed to be unknown and control input signals \mathcal{U}^{ID} are generated as a static sine wave with amplitude $4 \times 10^3 \text{ W}$

and period of one day. Such a control signal represents a constrained perturbation to the system dynamics with a similar purpose as a random sampling in the reinforcement learning setup. The disturbance signals \mathcal{D} represent the historical dataset of environmental conditions, namely solar irradiation, internal heat gains, and ambient temperature. The trajectories \mathcal{D} used for both system identification and control tasks are visualized at the bottom of Figure 2.

Control tasks: The objective of the control task is to do constrained off-policy optimization given only a small amount of measurement data of the system dynamics. To demonstrate the reference tracking capabilities during closed-loop control, the trajectory \mathcal{R} is generated as a static sine wave in range 18 °C to 22 °C and period of one day. However, for policy training, the trajectory \mathcal{R} is uniformly sampled in the realistic operative range of 15 °C to 25 °C to increase the generalization. The state and input constraints sequences $\underline{\mathcal{X}}, \overline{\mathcal{X}}, \underline{\mathcal{U}}, \overline{\mathcal{U}}$, are apriori defined. The simulated state trajectories, \mathcal{X} , are uniformly sampled state distribution in realistic range 0 °C to 25 °C to robustify the learned control policy. The control inputs trajectory \mathcal{U} is generated by the learned policies. For simultaneous system identification and control, the state and \mathcal{X}^{ID} , and inputs \mathcal{U}^{ID} trajectories are identical to those from the system identification task.

With a true model in hand, we could in principle generate an arbitrarily large dataset. However, we wish to demonstrate that our methods can operate in a data regime typical in the practical setting where only a fixed set of measurements over a limited time period is available. To this end, for all tasks, we run the ground truth simulation for a period of one month, with 5 minute sampling intervals giving a total of 288 samples per day and 2016 samples per week. The training, validation, and test sets are the 2nd, 3rd, and 4th weeks of simulation.

3.3. Metrics

We consider several metrics for assessing system identification and control policy performance. Our loss functions for training system models, the N -step prediction MSE (12), control MSE (16), and simultaneous system identification and control MSE (17) are expedient choices for optimization. However, a more robust indicator of success at the ultimate system identification task objective, to accurately simulate the dynamics of the system, is the MSE for an open-loop simulation over the entire test set. For a dataset with T total time steps, we define the open-loop MSE as: $\frac{1}{T} \sum_{k=1}^T \|\mathbf{x}_{k,4}^{\text{ID}} - \tilde{\mathbf{x}}_{k,4}\|_2^2$. Similarly, we use the closed-loop control simulation over the test set for performance assessment of learned control policy using the reference tracking MSE: $\frac{1}{T} \sum_{k=1}^T \|\mathbf{r}_k - \tilde{\mathbf{x}}_{k,4}\|_2^2$. The energy minimization term is evaluated as the mean absolute (MA) value of the

Table 1. Test set N -step MSE.

N	8	16	32	64	128	256
LIN	0.009	0.288	0.349	0.228	0.508	0.800
SSM	0.130	0.276	0.432	0.498	0.446	0.504
RNN	0.106	0.044	0.299	0.481	0.411	0.800
GRU	0.022	0.088	0.525	1.973	5.730	7.628

Table 2. Test set open-loop MSE.

N	8	16	32	64	128	256
LIN	1.685	0.472	1.134	1.023	0.350	1.071
SSM	5.374	1.331	0.938	0.469	0.446	0.313
RNN	2.585	5.634	1.462	1.437	0.884	1.071
GRU	157.3	3.904	3.904	8.292	14.22	6.844

control signal: $\frac{1}{T} \sum_{k=1}^T |\mathbf{u}_k|$. The state constraints violations are evaluated as MA value of the slack variables: $\frac{1}{T} \sum_{k=1}^T |\mathbf{s}_k^x|$.

3.4. System Identification

Table 1 shows the N -step MSE on the test set for each N -step prediction horizon training objective. The bold entries indicate the best performance for a given prediction horizon. We see that there is no single model which performs best for all N -step objectives. As N increases, models tend to higher N -step MSE. The GRU models show the greatest increase in N -step MSE according to N , whereas the SSM model shows far less tendency to gain error given longer prediction horizons.

Table 2 shows the open-loop MSE on the test set for models trained with each N -step prediction horizon. For all prediction horizons, either the SSM or simple linear model perform better on open-loop MSE, with the SSM achieving the best overall open-loop MSE when trained on the longest prediction horizon. In fact, for the SSM model we see an opposite trend from the N -step MSE, in that as N grows larger, models tend to do better at aligning the open-loop simulation with the reference trajectory. This makes sense for a well-posed model, as while modeling over larger spans of N is a more difficult learning objective, the larger N is, the closer the training objective is to the open-loop evaluation scenario. The absolute and percentage of reduction in open-loop MSE from the the contending LIN model (0.35 MSE) to the best performing SSM model (0.313 MSE) are 0.037 and 10% respectively. Performing a one-sided t -test for the LIN, SSM models on these squared prediction errors gives a p value of basically zero.

We investigate the practical import of performance gains by the trace of predicted state values for the best RNN, LIN,

Table 3. \mathbf{A} matrix system models eigenvalues.

	λ_1	λ_2	λ_3	λ_4
True	0.999	0.994	0.983	0.254
SSM	0.997	0.852	0.351	-0.005
LIN	0.997	0.385	$0.061 + 0.11i$	$0.061 - 0.11i$
RNN	0.996	0.293	$-0.260 + 0.05i$	$-0.256 - 0.05i$

and SSM models. Figure 1 shows the concatenated open-loop simulations from the training, validation and test sets, with the solid blue line indicating the true system trajectory. All models closely trace the path of the reference x_4 given only the initial state of the system and external inputs. Further, these models do well at staying in phase with the true trajectory for all variables except for x_3 . However, both the LIN and RNN models exhibit some clear bias for the x_2 variables with the RNN under- and the LIN over-estimating the true path. The RNN model is biased for all variables besides the reference. The GRU was able to train fairly reliably to track the N -step objective, however, for open-loop simulations, it failed to track even the reference x_4 , and is excluded due to out of scale performance.

Table 3 shows the eigenvalues of \mathbf{A} matrix for ground truth and learned dynamical models. Interestingly all models learned the dominant eigenvalue with high accuracy. However, the eigenvalues of the constrained SSM have the shortest Euclidean distance from those of the ground truth system. Moreover, the SSM is the only model learning non-complex eigenvalues, as is the case of the ground truth system. The physical interpretation of the real part of the complex eigenvalues represent scaling or gains of the system, while the imaginary part tells us about the frequencies of the generated signals (the larger the imaginary part, the larger the frequency). As a consequence, LIN and RNN models associate the periodic behavior of the training data with its main dynamics. However, this is not true as the periodicity of the training data is solely the results of the input \mathcal{U} and disturbance trajectories \mathcal{D} (day and night patterns). This observation provides an explanation why SSM outperforms LIN and RNN models in open-loop simulations.

3.5. Constrained Continuous Control

For continuous control task we train the proposed deep learning-based MPC (DLMPC) policy as defined in algorithm 1 with one-step ahead prediction horizon $N = 1$. The policy is trained with Adam optimizer [40] and learning rate of 0.001 on 30,000 epochs. The policy begins training with randomly initialized weights. We use the ground truth system model to demonstrate the potential of the policy learning algorithm. The different one week periods of 2016 samples are used as training, validation, and test sets, respectively. The weights of the loss function (16) are tuned using

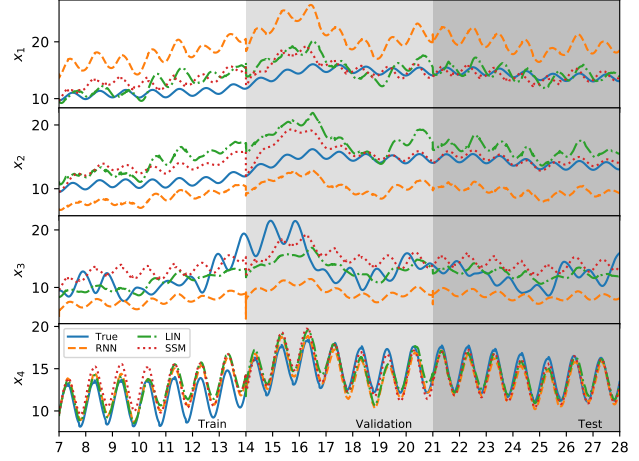


Figure 1. Open-loop simulation trajectories.

the physical insight about the system dynamics with the following values: $Q_r = 2e1$, $Q_u = 1e-6$, $Q_{su} = 5e-7$, $Q_{sx} = 5e1$. The results are reported on the test set. To assess the robustness of the trained policy we simulate the closed-loop with simulation model affected by parametric \mathbf{v}_k and additive \mathbf{w}_k uncertainties as follows:

$$\mathbf{x}_{k+1} = \mathbf{A}(\mathbf{v}_k)\mathbf{x}_k + \mathbf{B}\mathbf{u}_k + \mathbf{E}\mathbf{d}_k + \mathbf{w}_k, \quad (18)$$

where $\mathbf{v}_k \in \mathcal{N}(\mu_v, \sigma_v)$, $\mathbf{w}_k \in \mathcal{N}(\mu_w, \sigma_w)$ with $\mu_v = 0$, $\sigma_v = 0.01$, $\mu_w = 0$, and $\sigma_w = 0.1$.

We compare the performance of the trained DLMPC policy with classical model-based linear control methods, namely linear quadratic regulator (LQR), and Linear quadratic integral controller (LQI) implemented in Matlab environment using commands `dlqr` and `lqi`, respectively. The weights of LQI controller Q_r , and Q_u are chosen to be identical to the DLMPC policy, while tuning of the LQR weights was necessary to obtain satisfactory control results. The constraints penalties λ and μ do not apply to unconstrained classical control methods and are hence omitted.

Additionally, we evaluate the performance of three different formulations of model predictive control (MPC) problem. From the robustness perspective, we evaluate the performance of nominal deterministic MPC, worst-case robust MPC, and sampling-based stochastic MPC. The nominal MPC is obtained by the solution of the constrained optimization as defined by (13) with softened input and state constraints. Both robust and stochastic MPCs are designed to mitigate the effect of additive uncertainties \mathbf{w}_k . Robust MPC (RMPC) represents the worst-case scenario approach via constraints tightening techniques [61, 50] based on a priori defined bounds on the unknown disturbance. On the other hand, stochastic MPC (SMPC) is based on probabilistic constraints approximated by sampling from the known

distribution of the unknown disturbances. The implementation of RMPC and SMPC is based on the formulations presented in [23]. For a fair comparison, all MPC problems are designed with identical setup of the hyperparameters (N , Q_r , Q_u , λ , and μ) as in the case of trained DLMPC policy. The MPC problems are implemented in the Matlab environment using the Yalmip optimization toolbox [46]. Table 4 shows the closed-loop control performance of the investigated methods evaluated on the reference tracking MSE (MSE ref.), energy use (MA ene.), and constraints violation (MA en., MA con.) evaluated with various degrees of uncertainties \mathbf{v}_k and \mathbf{w}_k acting on the simulation model.

Table 4. Control performance on reference tracking, energy use, and constraints violations evaluated on closed-loop simulations with various degrees of uncertainties \mathbf{v}_k and \mathbf{w}_k . Evaluated controllers were learned/designed with the ground truth model.

Test set	No unc.	\mathbf{w}_k	\mathbf{v}_k	\mathbf{w}_k & \mathbf{v}_k
Proposed DLMPC policy				
MSE ref.	1.244	1.470	1.991	2.355
MA ene.	1111	1092	1177	1139
MA con.	0.000	0.000	0.000	0.000
Nominal MPC				
MSE ref.	1.398	1.785	3.343	3.711
MA ene.	897	847	917	866
MA con.	0.000	0.132	1.002	1.106
Robust MPC				
MSE ref.	1.405	1.640	2.727	2.839
MA ene.	899	892	910	836
MA con.	0.000	0.000	0.007	0.066
Stochastic MPC				
MSE ref.	1.398	1.422	2.238	3.579
MA ene.	897	995	977	856
MA con.	0.000	0.098	0.476	0.572
LQR				
MSE ref.	2.024	2.184	2.655	2.711
MA ene.	758	793	880	883
MA con.	5.574	6.550	7.362	7.567
LQI				
MSE ref.	1.954	2.544	3.399	4.957
MA ene.	899	861	920	676
MA con.	1.893	3.491	5.346	5.059

The results from Table 4 demonstrate a superior performance of the proposed DLMPC in the reference tracking against all compared methods while paying a cost in terms of increased energy use. While, the zero values of the constraints violations (MA con.) demonstrate that the learned DLMPC policy is capable of 100% constraints satisfaction also in the presence of parametric and additive uncertain-

ties, while simultaneously optimizing the reference tracking objective. In terms of constraints satisfaction it also outperforms all compared control approaches. These results indicate that the proposed state-space sampling-based method is a competitive alternative to constraints tightening-based robust MPC and stochastic MPC based on a sampling of additive uncertainties. An interesting observation is that while using the same hyperparameters as all MPC variants, the proposed DLMPC method favors the constraints satisfaction and tracking performance before the energy use minimization. This can be explained by the state space and reference trajectory sampling stimulating the policy to learn robust behavior across a variety of initial conditions and reference signals. As expected, the performance of the LQR and LQI on the given control task is unsatisfactory, as these classical control approaches are not designed to handle control problems with inequality constraints.

3.6. Simultaneous System Identification and Control

For the simultaneous system identification and constrained control learning task we train the parametrized model as defined in algorithm 2 with one-step ahead prediction horizon $N = 1$. The model is trained with Adam optimizer with learning rate of 0.001 on 40,000 epochs. The system model and the policy begin training with randomly initialized weights. The same train, validation, and test sets are used as described in section 3.5. The weights of the loss function (17) for the control part remain unchanged as given in section 3.5, the modeling weights are: $Q_{ID} = 1e2$, $Q_{\Delta x} = 1e0$. The results are reported on the test set. The simulation model during the closed-loop control is affected by uncertainties as defined via eq. (18). To demonstrate the adaptive capabilities of the policy we apply the online updates with optimization over 10 epochs only during the test set.

Table 5 shows the closed-loop control performance of the adaptive DLMPC policy evaluated on the modeling MSE (MSE mod.), reference tracking MSE (MSE ref.), energy use (MA ene.), and constraints violation (MA en., MA con.) for trained policy with learned model evaluated on 20 simulation runs. Interestingly, the performance in terms of the constraint satisfaction is comparable to robust MPC designed with the ground truth model, while being significantly less conservative in terms of reference tracking having superior performance across all investigated control approaches. The performance of the joint model and policy learning, together with the corrective effects of the adaptive model and updates during online evaluation demonstrate the competitive nature of the proposed methodology compared to classical approaches. The non-zero values of MSE for the model and reference tracking are caused by hard constraints on states and control actions, causing situations when the reference trajectory is not reachable. Such a scenario was deliberately

Table 5. Closed-loop control performance on model prediction, reference tracking, energy use, and constraints violations of simultaneous model and policy learning evaluated on closed-loop simulations with various degrees of uncertainties \mathbf{v}_k and \mathbf{w}_k .

Test set	No unc.	\mathbf{w}_k	\mathbf{v}_k	\mathbf{w}_k & \mathbf{v}_k
MSE mod.	0.344	0.485	1.325	1.781
MSE ref.	0.952	1.126	2.263	2.932
MA ene.	1102	1139	1134	1109
MA con.	0.000	0.002	0.014	0.053

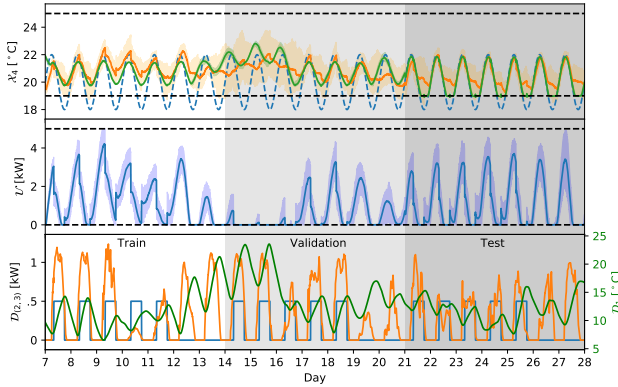


Figure 2. Closed-loop control simulation trajectories of simultaneous system identification and adaptive policy learning.

chosen and showed that the learned policy deems state and input constraints satisfaction a superior task due to large constraints violation penalties. Hence, the policy may sacrifice control performance in situations when constraints could be compromised.

Figure 2 shows the closed-loop simulations for the training, validation and test sets with simulation model affected by additive uncertainty \mathbf{w}_k . The upper plot shows the trajectories of the controlled (orange) and learned predicted (green) state. The middle plot shows control’s policy actions, while the bottom plot shows the influence of measured disturbances. Error bars represent the influence of various realizations of uncertainties. The plots demonstrate that the DLMPC policy can consistently predict the trajectory and track the reference of a controlled state while satisfying the state and input constraints most of the time. Please note that parts of the reference trajectory (dashed blue) were deliberately chosen to be outside the state constraints (dashed black) to demonstrate the balancing capabilities of the multi-objective loss (17). Online learning was active only during the test set and decreased the difference between predicted (green) and controlled (orange) state, as well as the variance of the controlled (orange) state. As a consequence, the constraints handling is also improved with online updates.

Table 6. Scalability with increasing prediction horizon N . Comparison of mean and worst case online computational time per sample, and memory footprint of the proposed deep learning-based strategy (DLMPC) with implicit (iMPC) and explicit (eMPC) solutions.

N	1	2	4	6	8
mean CPU time [$1e^{-3}$ s]					
DLMPC	0.37	0.60	1.03	1.50	1.92
eMPC	0.15	0.45	4.04	9.48	–
iMPC	3.00	7.86	10.52	10.31	8.53
max CPU time [$1e^{-3}$ s]					
DLMPC	9.94	15.93	10.06	11.73	10.19
eMPC	6.00	10.00	23.00	82.00	–
iMPC	53.00	40.00	68.00	73.00	92.00
memory footprint [kB]					
DLMPC	9.18	8.96	11.60	15.80	21.60
eMPC	48.00	1051	7523	35176	458671
iMPC ¹	~150	~150	~150	~150	~150

Similarly to LQR and MPC, the proposed DLMPC policy is a full state feedback controller. Therefore a state estimator is necessary for practical applications with partially observable systems. Fortunately, the learned model can be used for the design of the Kalman filter or Moving horizon estimator (MHE). An alternative approach would be the use of autoregressive state-space model based on the system measurements.

3.7. Computational Aspects and Scalability

From the computational and memory standpoint we compare the proposed method with implicit and explicit solutions of the MPC problems. The implicit problem is solved online via quadratic programming (QP) using Matlab’s Quadprog solver [25]. While, the explicit problem is solved offline via multiparametric quadratic programming (mpQP) using MPT3 toolbox [34]. Upon deployment, the online explicit MPC procedure consists of an evaluation of a pre-computed piecewise affine (PWA) policy. The online computation time and memory footprints of the investigated control policies were evaluated on a laptop with 2.60 GHz Intel(R) i7-8850H CPU and 16 GB RAM on a 64-bit operating system. The assessment of the memory requirements of the implicit MPC is not straightforward, as it depends on the memory footprint of the chosen optimization solver, dependencies, and storage of the problem parameters. In this case, we estimate the optimistic lower bound by assessing only the memory requirements of the Quadprog solver².

In general, the complexity of the QP problem depends on

²The memory footprint estimate of implicit MPC in Table 6 is based on the standalone Python implementation of the Quadprog solver: <https://pypi.org/project/quadprog/>

the number of possible combinations of active constraints, which scale exponentially with the prediction horizon steps N , the number of states, and decision variables. The Table 6 demonstrates the scalability analysis of the mean and worst-case evaluation time, and memory footprint as a function of increasing prediction horizon N . We train two layer DLMPC policy, with increasing number of hidden layers $n_{\text{hidden}} = 10N$. DLMPC and iMPC policies share the same hyperparameters, however, due to the exponential complexity growth in the case of eMPC we had to implement the move blocking strategy [15] limiting the length of the control horizon for prediction horizons larger than 4 as follows: if $N = 4$ then $N_c = 2$, and if $N = 6$ then $N_c = 1$, while the problem with $N = 8$ is practically intractable even with $N_c = 1$. The results show that the learned DLMPC policy is on average 5 to 10 times faster than iMPC policy, with 7 to 15 times smaller memory footprint. In comparison with eMPC, the DLMPC has significantly smaller memory footprint across all scales. Both CPU time as well as memory footprint of the DLMPC policies scale linearly with the problem complexity, while eMPC solutions scale exponentially and are practically infeasible for larger scale problems. These findings are supported by the analytical analysis showing that DNNs with ReLU layers are much more memory efficient than lookup tables for parametrizing the PWA functions representing eMPC policies [39]. Moreover, the online complexity of DLMPC depends entirely on the choice of the policy parametrizations, i.e., number of layers, and hidden neurons. Therefore it can represent a tunable trade-off between the performance and guaranteed complexity, a design trait desirable in particular for embedded applications with limited computational resources.

4. Conclusions and Future Work

In this work we present control methods bridging physics-based and learning-based approaches. Our methods are able to learn a linear dynamics model given limited data, and to leverage the simulated behavior for policy optimization. The stability of the linear model and well-posedness of the associated learning problem are guaranteed by RNN cells which incorporate prior physical knowledge about the system dynamics based on eigenvalue analysis. We demonstrate the use of barrier methods for the encoding of equality and inequality constraints within deep learning models, ensuring safe control. Weighted multi-objective loss functions balance various possibly competing objectives of process control and system constraints. The system model, as well as the policy, are learned end-to-end without the need for an expert policy to imitate. Moreover, the model is capable of learning from static datasets without the need for active system perturbation.

The performance of the proposed method was compared

with a variety of traditional control methods, in particular LQR and LQI controllers, three variants of MPC formulations, and two solution alternatives to the associated constrained optimization problem. The case study compared the performance on reference tracking loss, energy minimization, robustness to uncertainties, and computational scalability with increasing prediction horizon. Based on the presented results and user-friendly end-to-end training, we believe that the proposed methodology has the potential to be deployed in the application domains beyond the computational reach of the traditional MPC approaches based on the online solution of quadratic programs (QP) or offline solutions of the multi parametric quadratic programs (mpQP).

The proposed paper presents a proof of concept and preliminary analysis of the performance of the proposed methodology. The main limitation of this study is the demonstration of a small scale fully observable linear system. Therefore, the performance on a large-scale linear system, different systems with partially observable state spaces, and extensions to non-linear dynamics will be addressed in the future work.

Acknowledgements

This work has been supported by the U.S. Department of Energy’s (DOE) Building Technologies Office, Emerging Technologies Program.

References

- [1] Agrawal, A., Amos, B., Barratt, S., Boyd, S., Diamond, S., and Kolter, Z. Differentiable convex optimization layers. *ArXiv*, abs/1910.12430, 2019.
- [2] Alessio, A. and Bemporad, A. *A Survey on Explicit Model Predictive Control, in Nonlinear Model Predictive Control: Towards New Challenging Applications*, pp. 345–369. Springer Berlin Heidelberg, Berlin, Heidelberg, 2009. ISBN 978-3-642-01094-1.
- [3] Amos, B., Xu, L., and Kolter, J. Z. Input convex neural networks. *CoRR*, abs/1609.07152, 2016. URL <http://arxiv.org/abs/1609.07152>.
- [4] Amos, B., Rodriguez, I. D. J., Sacks, J., Boots, B., and Kolter, J. Z. Differentiable MPC for end-to-end planning and control. *CoRR*, abs/1810.13400, 2018. URL <http://arxiv.org/abs/1810.13400>.
- [5] Asarin, E., Bournez, O., Dang, T., and Maler, O. Approximate reachability analysis of piecewise-linear dynamical systems. In Lynch, N. and Krogh, B. H. (eds.), *Hybrid Systems: Computation and Control*, pp. 20–31,

Berlin, Heidelberg, 2000. Springer Berlin Heidelberg. ISBN 978-3-540-46430-3.

- [6] Aswani, A., Gonzalez, H., Sastry, S. S., and Tomlin, C. Provably safe and robust learning-based model predictive control. *Automatica*, 49(5):1216 – 1226, 2013. ISSN 0005-1098. doi: <https://doi.org/10.1016/j.automatica.2013.02.003>. URL <http://www.sciencedirect.com/science/article/pii/S0005109813000678>.
- [7] Aswani, A., Bouffard, P., Zhang, X., and Tomlin, C. Practical comparison of optimization algorithms for learning-based mpc with linear models, 2014.
- [8] Behrmann, J., Duvenaud, D., and Jacobsen, J. Invertible residual networks. *CoRR*, abs/1811.00995, 2018. URL <http://arxiv.org/abs/1811.00995>.
- [9] Bemporad, A., Borrelli, F., and Morari, M. Explicit solution of LP-based model predictive control. In *CDC*, Sydney, Australia, December 2000.
- [10] Ben-Tal, A. and Nemirovski, A. *Lectures on Modern Convex Optimization: Analysis, Algorithms, and Engineering Applications*. MPS/SIAM Series on Optimization. SIAM, 2001.
- [11] Bieker, K., Peitz, S., Brunton, S. L., Kutz, J. N., and Dellnitz, M. Deep model predictive control with online learning for complex physical systems. *CoRR*, abs/1905.10094, 2019. URL <http://arxiv.org/abs/1905.10094>.
- [12] Boyd, S. and Vandenberghe, L. *Convex Optimization*. Cambridge University Press, 2004.
- [13] Broad, A., Abraham, I., Murphey, T. D., and Argall, B. D. Structured neural network dynamics for model-based control. *CoRR*, abs/1808.01184, 2018. URL <http://arxiv.org/abs/1808.01184>.
- [14] Bujarbaruah, M., Zhang, X., Rosolia, U., and Borrelli, F. Adaptive mpc for iterative tasks. *2018 IEEE Conference on Decision and Control (CDC)*, pp. 6322–6327, 2018.
- [15] Cagienard, R., Grieder, P., Kerrigan, E., and Morari, M. Move Blocking Strategies in Receding Horizon Control. *Journal of Process Control*, 17(6):563–570, July 2007.
- [16] Chen, S. W., Wang, T., Atanasov, N., Kumar, V., and Morari, M. Large scale model predictive control with neural networks and primal active sets, 2019.
- [17] Chen, T. Q., Rubanova, Y., Bettencourt, J., and Duvenaud, D. K. Neural ordinary differential equations. In Bengio, S., Wallach, H., Larochelle, H., Grauman, K., Cesa-Bianchi, N., and Garnett, R. (eds.), *Advances in Neural Information Processing Systems 31*, pp. 6571–6583. Curran Associates, Inc., 2018.
- [18] Chen, Y., Shi, Y., and Zhang, B. Optimal control via neural networks: A convex approach, 2018.
- [19] Christiano, P. F., Shah, Z., Mordatch, I., Schneider, J., Blackwell, T., Tobin, J., Abbeel, P., and Zaremba, W. Transfer from simulation to real world through learning deep inverse dynamics model. *CoRR*, abs/1610.03518, 2016. URL <http://arxiv.org/abs/1610.03518>.
- [20] Chung, J., Gulcehre, C., Cho, K., and Bengio, Y. Empirical evaluation of gated recurrent neural networks on sequence modeling. *arXiv preprint arXiv:1412.3555*, 2014.
- [21] de Avila Belbute-Peres, F., Smith, K., Allen, K., Tenenbaum, J., and Kolter, J. Z. End-to-end differentiable physics for learning and control. In Bengio, S., Wallach, H., Larochelle, H., Grauman, K., Cesa-Bianchi, N., and Garnett, R. (eds.), *Advances in Neural Information Processing Systems 31*, pp. 7178–7189. Curran Associates, Inc., 2018.
- [22] Degraeve, J., Hermans, M., Dambre, J., and Wyffels, F. A differentiable physics engine for deep learning in robotics. *CoRR*, abs/1611.01652, 2016. URL <http://arxiv.org/abs/1611.01652>.
- [23] Dragoňa, J., Kvasnica, M., Klaučo, M., and Fikar, M. Explicit Stochastic MPC Approach to Building Temperature Control. In *IEEE Conference on Decision and Control*, pp. 6440–6445, Florence, Italy, 2013.
- [24] Dulac-Arnold, G., Mankowitz, D. J., and Hester, T. Challenges of real-world reinforcement learning. *CoRR*, abs/1904.12901, 2019. URL <http://arxiv.org/abs/1904.12901>.
- [25] Goldfarb, D. and Idnani, A. U. A numerically stable dual method for solving strictly convex quadratic programs. *Mathematical Programming*, 27:1–33, 1983.
- [26] Greydanus, S., Dzamba, M., and Yosinski, J. Hamiltonian neural networks. *CoRR*, abs/1906.01563, 2019. URL <http://arxiv.org/abs/1906.01563>.
- [27] Grötschel, M., Krumke, S. O., and Rambau, J. (eds.). *Introduction to Model Based Optimization of Chemical Processes on Moving Horizons*, pp. 295–339. Springer Berlin Heidelberg, Berlin, Heidelberg, 2001. ISBN 978-3-662-04331-8. doi: 10.1007/978-3-662-04331-8.18. URL https://doi.org/10.1007/978-3-662-04331-8_18.

- [28] Haber, E. and Ruthotto, L. Stable architectures for deep neural networks. *CoRR*, abs/1705.03341, 2017. URL <http://arxiv.org/abs/1705.03341>.
- [29] Haber, E., Lensink, K., Treister, E., and Ruthotto, L. IMEXnet: A forward stable deep neural network. *CoRR*, abs/1903.02639, 2019. URL <http://arxiv.org/abs/1903.02639>.
- [30] Hafner, D., Lillicrap, T. P., Fischer, I., Villegas, R., Ha, D., Lee, H., and Davidson, J. Learning latent dynamics for planning from pixels. *CoRR*, abs/1811.04551, 2018. URL <http://arxiv.org/abs/1811.04551>.
- [31] Hafner, D., Lillicrap, T., Ba, J., and Norouzi, M. Dream to control: Learning behaviors by latent imagination, 2019.
- [32] He, K., Zhang, X., Ren, S., and Sun, J. Deep residual learning for image recognition. *CoRR*, abs/1512.03385, 2015. URL <http://arxiv.org/abs/1512.03385>.
- [33] Heess, N., Wayne, G., Silver, D., Lillicrap, T. P., Tassa, Y., and Erez, T. Learning continuous control policies by stochastic value gradients. *CoRR*, abs/1510.09142, 2015. URL <http://arxiv.org/abs/1510.09142>.
- [34] Herceg, M., Kvasnica, M., Jones, C., and Morari, M. Multi-parametric toolbox 3.0. In *2013 European Control Conference, Zurich, Switzerland*, pp. 502–510, 2013.
- [35] Hertneck, M., Köhler, J., Trimpe, S., and Allgöwer, F. Learning an approximate model predictive controller with guarantees. *CoRR*, abs/1806.04167, 2018. URL <http://arxiv.org/abs/1806.04167>.
- [36] Hewing, L., Wabersich, K. P., Menner, M., and Zeilinger, M. N. Learning-based model predictive control: Toward safe learning in control. *Annual Review of Control, Robotics, and Autonomous Systems*, 3(1):null, 2020. doi: 10.1146/annurev-control-090419-075625. URL <https://doi.org/10.1146/annurev-control-090419-075625>.
- [37] Izzo, D., Taylor, D., and Vasileiou, T. On the stability analysis of optimal state feedbacks as represented by deep neural models. *CoRR*, abs/1812.02532, 2018. URL <http://arxiv.org/abs/1812.02532>.
- [38] Jeen-Shing Wang and Yi-Chung Chen. A hammerstein-wiener recurrent neural network with universal approximation capability. In *2008 IEEE International Conference on Systems, Man and Cybernetics*, pp. 1832–1837, Oct 2008. doi: 10.1109/ICSMC.2008.4811555.
- [39] Karg, B. and Lucia, S. Efficient representation and approximation of model predictive control laws via deep learning, 2018.
- [40] Kingma, D. P. and Ba, J. Adam: A method for stochastic optimization. *arXiv preprint arXiv:1412.6980*, 2014.
- [41] Knill, O. *Linear Algebra with Probability*. Harvard College Course Math 19b, 2011.
- [42] Kolter, J. Z. and Manek, G. Learning stable deep dynamics models. In Wallach, H., Larochelle, H., Beygelzimer, A., d Alch-Buc, F., Fox, E., and Garnett, R. (eds.), *Advances in Neural Information Processing Systems* 32, pp. 11126–11134. Curran Associates, Inc., 2019. URL <http://papers.nips.cc/paper/9292-learning-stable-deep-dynamics-models.pdf>.
- [43] Krishnan, R. G., Shalit, U., and Sontag, D. Deep kalman filters, 2015.
- [44] Krishnan, R. G., Shalit, U., and Sontag, D. Structured inference networks for nonlinear state space models, 2016.
- [45] Kvasnica, M. *Real-Time Model Predictive Control via Multi-Parametric Programming: Theory and Tools*. VDM Verlag, Saarbruecken, January 2009.
- [46] Löfberg, J. YALMIP : A Toolbox for Modeling and Optimization in MATLAB. In *Proc. of the CACSD Conference*, Taipei, Taiwan, 2004. Available from <http://users.isy.liu.se/johanl/yalmip/>.
- [47] Loshchilov, I. and Hutter, F. Decoupled weight decay regularization. *arXiv preprint arXiv:1711.05101*, 2017.
- [48] Lu, L., Meng, X., Mao, Z., and Karniadakis, G. E. DeepXDE: A deep learning library for solving differential equations. *CoRR*, abs/1907.04502, 2019. URL <http://arxiv.org/abs/1907.04502>.
- [49] Lutter, M., Ritter, C., and Peters, J. Deep lagrangian networks: Using physics as model prior for deep learning. *CoRR*, abs/1907.04490, 2019. URL <http://arxiv.org/abs/1907.04490>.
- [50] Löfberg, J. Minimax approaches to robust model predictive control, 2003.
- [51] Maciejowski, J. M. *Predictive Control with Constraints*. Prentice Hall, 2002. ISBN 0-201-39823-0.

- [52] Mordatch, I. and Todorov, E. Combining the benefits of function approximation and trajectory optimization. In *In Robotics: Science and Systems (RSS)*, 2014.
- [53] Paszke, A., Gross, S., Massa, F., Lerer, A., Bradbury, J., Chanan, G., Killeen, T., Lin, Z., Gimelshein, N., Antiga, L., et al. Pytorch: An imperative style, high-performance deep learning library. In *Advances in Neural Information Processing Systems*, pp. 8024–8035, 2019.
- [54] Puskorius, G. and Feldkamp, L. Truncated backpropagation through time and Kalman filter training for neurocontrol. In *Proceedings of 1994 IEEE International Conference on Neural Networks (ICNN'94)*, volume 4, pp. 2488–2493. IEEE, 1994.
- [55] Rakovic, S. V., Kerrigan, E. C., Mayne, D. Q., and Lygeros, J. Reachability analysis of discrete-time systems with disturbances. *IEEE Transactions on Automatic Control*, 51(4):546–561, April 2006. ISSN 2334-3303. doi: 10.1109/TAC.2006.872835.
- [56] Rangapuram, S. S., Seeger, M. W., Gasthaus, J., Stella, L., Wang, Y., and Januschowski, T. Deep state space models for time series forecasting. In Bengio, S., Wallach, H., Larochelle, H., Grauman, K., Cesa-Bianchi, N., and Garnett, R. (eds.), *Advances in Neural Information Processing Systems 31*, pp. 7785–7794. Curran Associates, Inc., 2018.
- [57] Richards, S. M., Berkenkamp, F., and Krause, A. The Lyapunov neural network: Adaptive stability certification for safe learning of dynamic systems. *CoRR*, abs/1808.00924, 2018. URL <http://arxiv.org/abs/1808.00924>.
- [58] Sanchez-Gonzalez, A., Heess, N., Springenberg, J. T., Merel, J., Riedmiller, M. A., Hadsell, R., and Battaglia, P. W. Graph networks as learnable physics engines for inference and control. *CoRR*, abs/1806.01242, 2018. URL <http://arxiv.org/abs/1806.01242>.
- [59] Sanchez-Gonzalez, A., Bapst, V., Cranmer, K., and Battaglia, P. Hamiltonian graph networks with ode integrators, 2019.
- [60] Sanchez-Gonzalez, A., Godwin, J., Pfaff, T., Ying, R., Leskovec, J., and Battaglia, P. W. Learning to simulate complex physics with graph networks, 2020.
- [61] Schuurmans, J. and Rossiter, J. A. Robust predictive control using tight sets of predicted states. *Control Theory and Applications*, 147:13–18, 2000.
- [62] Soloperto, R., Müller, M. A., Trimpe, S., and Allgöwer, F. Learning-based robust model predictive control with state-dependent uncertainty. *IFAC-PapersOnLine*, 51(20):442 – 447, 2018. ISSN 2405-8963. doi: <https://doi.org/10.1016/j.ifacol.2018.11.052>. URL <http://www.sciencedirect.com/science/article/pii/S2405896318327101>. 6th IFAC Conference on Nonlinear Model Predictive Control NMPC 2018.
- [63] Tøndel, P., Johansen, T. A., and Bemporad, A. An Algorithm for Multi-Parametric Quadratic Programming and Explicit MPC Solutions. *aut*, November 2001. Preprint submitted.
- [64] Ushida, D. and Konaka, E. Model predictive control implementation on neural networks using denoising autoencoder. In *2016 IEEE International Conference on Systems, Man, and Cybernetics (SMC)*, pp. 000149–000154, Oct 2016. doi: 10.1109/SMC.2016.7844234.
- [65] Wills, A. G. and Heath, W. P. Barrier function based model predictive control. *Automatica*, 40(8):1415 – 1422, 2004. ISSN 0005-1098. doi: <https://doi.org/10.1016/j.automatica.2004.03.002>. URL <http://www.sciencedirect.com/science/article/pii/S0005109804000809>.
- [66] Yu Wang. A new concept using lstm neural networks for dynamic system identification. In *2017 American Control Conference (ACC)*, pp. 5324–5329, 2017.
- [67] Zhang, T., Kahn, G., Levine, S., and Abbeel, P. Learning deep control policies for autonomous aerial vehicles with MPC-guided policy search. *CoRR*, abs/1509.06791, 2015. URL <http://arxiv.org/abs/1509.06791>.
- [68] Zhang, X., Bujarbaruah, M., and Borrelli, F. Safe and near-optimal policy learning for model predictive control using primal-dual neural networks. *2019 American Control Conference (ACC)*, pp. 354–359, 2019.
- [69] Zhang, X., Bujarbaruah, M., and Borrelli, F. Near-optimal rapid mpc using neural networks: A primal-dual policy learning framework, 2019.